Draft version June 20, 2014
Preprint typeset using LaTeX style emulateapj v. 04/17/13

arXiv:1403.1496v1 [astro-ph.GA] 6 Mar 2014

EVOLUTION OF THE FRACTION OF CLUMPY GALAXIES AT $0.2 < Z < 1.0$ IN THE COSMOS FIELD*

K. L. Murata[1,2], M. Kajisawa[2,3], Y. Taniguchi[3], M. A. R. Kobayashi[3], Y. Shioya[3], P. Capak[4], O. Ilbert[5], A. M. Koekemoer[6], M. Salvato[7], N. Z. Scoville[8]

Draft version June 20, 2014

ABSTRACT

Using the *Hubble Space Telescope*/Advanced Camera for Surveys data in the COSMOS field, we systematically searched clumpy galaxies at $0.2 < z < 1.0$ and investigated the fraction of clumpy galaxies and its evolution as a function of stellar mass, star formation rate (SFR), and specific SFR (SSFR). The fraction of clumpy galaxies in star-forming galaxies with $M_{\rm star} > 10^{9.5} M_{\odot}$ decreases with time from ~ 0.35 at $0.8 < z < 1.0$ to ~ 0.05 at $0.2 < z < 0.4$ irrespective of the stellar mass, although the fraction tends to be slightly lower for massive galaxies with $M_{\rm star} > 10^{10.5} M_{\odot}$ at each redshift. On the other hand, the fraction of clumpy galaxies increases with increasing both SFR and SSFR in all the redshift ranges we investigated. In particular, we found that the SSFR dependences of the fractions are similar among galaxies with different stellar masses, and the fraction at a given SSFR does not depend on the stellar mass in each redshift bin. The evolution of the fraction of clumpy galaxies from $z \sim 0.9$ to $z \sim 0.3$ seems to be explained by such SSFR dependence of the fraction and the evolution of SSFRs of star-forming galaxies. The fraction at a given SSFR also appears to decrease with time, but this can be due to the effect of the morphological K-correction. We suggest that these results are understood by the gravitational fragmentation model for the formation of giant clumps in disk galaxies, where the gas mass fraction is a crucial parameter.

Subject headings: galaxies: evolution — galaxies: irregular — galaxies: star formation

1. INTRODUCTION

In the present universe, most bright galaxies have regular and symmetric morphologies, which can be classified in the framework of the Hubble sequence (Hubble 1936). On the other hand, using the high-resolution imaging capability of the *Hubble Space Telescope* (*HST*), it has been found that many star-forming galaxies at $z > 1$ have irregular shapes with asymmetric structures, (e.g., Cowie et al. 1995; Steidel et al. 1996; Kajisawa & Yamada 2001; Elmegreen et al. 2007; Cameron et al. 2011). Although these high-redshift irregular galaxies show a variety of morphologies, they commonly have giant (kpc scale) star-forming clumps (e.g., Elmegreen et al. 2009a; Förster Schreiber et al. 2011). Recent NIR integral field spectroscopy observations of star-forming clumpy galaxies at $z \sim 2$ revealed that a significant fraction of these galaxies show coherent rotation with a relatively large turbulent velocity in their ionized gas kinematics (e.g., Förster Schreiber et al. 2006; Wright et al. 2007; Genzel et al. 2008; Cresci et al. 2009; Förster Schreiber et al. 2009). Several studies of the radio CO line observations also found that actively star-forming galaxies at $1 \lesssim z \lesssim 3$ have large gas mass fractions of $\sim 0.3 - 0.8$ (Daddi et al. 2010; Tacconi et al. 2010; Tacconi et al. 2013). While some of these galaxies are galaxy mergers (e.g., Somerville et al. 2001; Lotz et al. 2004; Puech 2010), these results can be explained by theoretical models where gas-rich rotational disks are gravitationally unstable for the fragmentation and lead to the formation of giant star-forming clumps (e.g., Noguchi 1998; Immeli et al. 2004; Bournaud et al. 2007; Dekel et al. 2009a). The high gas mass fraction of these galaxies is considered to be maintained by the rapid and smooth cosmic infall of gas along large-scale filaments. Since the accretion rate of gas is expected to decrease with time, especially at $z \lesssim 1$, the gas fraction of these clumpy galaxies declines at lower red-

* Based on observations with the NASA/ESA *Hubble Space Telescope*, obtained at the Space Telescope Science Institute, which is operated by AURA Inc, under NASA contract NAS 5-26555. Also based on observations made with the Spitzer Space Telescope, which is operated by the Jet Propulsion Laboratory, California Institute of Technology, under NASA contract 1407. Also based on data collected at; the Subaru Telescope, which is operated by the National Astronomical Observatory of Japan; the XMM-Newton, an ESA science mission with instruments and contributions directly funded by ESA Member States and NASA; the European Southern Observatory under Large Program 175.A-0839, Chile; Kitt Peak National Observatory, Cerro Tololo Inter-American Observatory and the National Optical Astronomy Observatory, which are operated by the Association of Universities for Research in Astronomy, Inc. (AURA) under cooperative agreement with the National Science Foundation; and the Canada-France-Hawaii Telescope with MegaPrime/MegaCam operated as a joint project by the CFHT Corporation, CEA/DAPNIA, the NRC and CADC of Canada, the CNRS of France, TERAPIX and the Univ. of Hawaii.

[1] Department of Particle and Astrophysical Science, Nagoya University, Furo-cho, Chikusa-ku, Nagoya 464-8602, Japan *e-mail murata.katsuhiro@g.mbox.nagoya-u.ac.jp*
[2] Graduate School of Science and Engineering, Ehime University, Bunkyo-cho, Matsuyama 790-8577, Japan
[3] Research Center for Space and Cosmic Evolution, Ehime University, Bunkyo-cho, Matsuyama 790-8577, Japan
[4] Spitzer Science Center, 314-6 Caltech, Pasadena, CA 91125, USA
[5] Aix Marseille Université, CNRS, LAM (Laboratoire d'Astrophysique de Marseille), UMR 7326, 13388, Marseille, France
[6] Space Telescope Science Institute, 3700 San Martin Drive, Baltimore, MD 21218, USA
[7] Max Planck Institut für Plasma Physik and Excellence Cluster, 85748 Garching, Germany
[8] California Institute of Technology, MC 249-17, 1200 East California Boulevard, Pasadena, CA 91125, USA

shifts as the gas consumption by the star formation proceeds, which results in the stabilization of the gas disks (Cacciato et al. 2012). In this view, these high-redshift clumpy galaxies are considered to be progenitors of normal (disk) galaxies at low redshifts. Therefore, it is important to study the evolution of these clumpy galaxies in order to understand the formation process of normal galaxies in the present universe.

However, the number of systematic surveys for clumpy galaxies is very limited, because wide-field imaging data with high spatial resolution are required. While Elmegreen et al. (2007) claimed that clumpy galaxies are dominated at high redshift based on the morphological analysis of galaxies in the HUDF field, Tadaki et al. (2014) reported that ∼40% of 100 Hα emitters at $z \sim 2.2$ and $z \sim 2.5$ in the UKIDSS/UDS-CANDELS field show clumpy morphologies. Wuyts et al. (2012) measured the fraction of clumpy galaxies in star-forming galaxies with $M_{\rm star} > 10^{10} M_{\odot}$ at $z \sim 2$ in the GOODS-South field, and found that the fraction is 74% for clumps selected at the rest-frame 2800 Å and 42% for those selected at the rest-frame V band, which suggests that the morphological K-correction can be important for the selection of clumpy galaxies. Although systematic surveys of clumpy galaxies at lower redshifts are also important for understanding the connection between clumpy galaxies at high redshifts and normal galaxies in the nearby universe, there is few survey for clumpy galaxies at $z \lesssim 1$. In this paper, we systematically search clumpy galaxies at $0.2 < z < 1.0$ in the COSMOS field (Scoville et al. 2007) and investigate their physical properties. The high spatial resolution images taken with *HST*/Advanced Camera for Surveys (ACS) over the very wide field allow us to construct a large sample of clumpy galaxies at $z < 1$ and to investigate the fraction of clumpy galaxies and its evolution as a function of physical properties such as stellar mass and star formation rate for the first time. Section 2 describes our sample and details of the selection method for clumpy galaxies. We present the physical properties of clumpy galaxies and investigate the fraction of these galaxies and its evolution in Section 3. In Section 4, we summarize our results and discuss their implications. Throughout this paper, magnitudes are given in the AB system. We adopt a flat universe with $\Omega_{\rm matter} = 0.3$, $\Omega_{\Lambda} = 0.7$, and $H_0 = 70$ km s^{-1} Mpc^{-1}.

2. SAMPLE AND ANALYSIS

2.1. *Sample*

In this study, we used a sample of galaxies with photometric redshifts of $0.2 < z < 1.0$ from the COSMOS photometric redshift catalog (Ilbert et al. 2009). We basically analyzed galaxies with $I_{\rm F814W} < 22.5$ in order to securely select clumpy galaxies in the *HST*/ACS $I_{\rm F814W}$-band images (see the next subsection). The photometric redshift is estimated with more than 30 bands data from UV to MIR wavelength in the COSMOS field, and its uncertainty is very small ($\Delta z \lesssim 0.02$) for galaxies with $I_{\rm F814W} < 22.5$ at $z < 1$ (Ilbert et al. 2009), which is sufficiently accurate for our purpose.

In order to investigate the fraction of clumpy galaxies as a function of the physical properties of galaxies, we used the stellar mass ($M_{\rm star}$) and the star formation rate (SFR) of our sample galaxies estimated from the spectral energy distribution (SED) fitting technique (Ilbert et al. 2010; Ilbert et al. 2013). The multi-band photometric data from UV to MIR wavelength were fitted with the population synthesis model by Bruzual & Charlot (2003). The exponentially declining star formation histories and the Calzetti et al. (2000) extinction law were assumed, and the Chabrier (2003) IMF was adopted (see Ilbert et al. 2013 for details). The best-fit model was used to convert the luminosities to the stellar mass and the SFR. We excluded X-ray sources detected in the *Chandra* or *XMM-Newton* images (Hasinger et al. 2007; Elvis et al. 2009) and galactic stars classified in the SED fitting from our sample.

TABLE 1
Number of galaxies in our sample

Redshift	All ($M_{\rm star} > 10^{9.5} M_{\odot}$)	Clumpy ($M_{\rm star} > 10^{9.5} M_{\odot}$)
$0.2 \leq z < 0.4$	7392 (3826)	363 (106)
$0.4 \leq z < 0.6$	5742 (4221)	464 (304)
$0.6 \leq z < 0.8$	6297 (5597)	895 (781)
$0.8 \leq z < 1.0$	4596 (4500)	1081 (1055)
total	24027 (18144)	2803 (2246)

2.2. *Selection for Clumpy Galaxies*

Using the *HST*/ACS $I_{\rm F814W}$-band data of the COSMOS survey (version 2.0, Koekemoer et al. 2007), we examined the morphology of our sample galaxies and selected clumpy galaxies quantitatively. The pixel scale of the reduced ACS images is 0.03 arcsec and the FWHM of the Point Spread Function is ∼ 0.1 arcsec. The clumpy galaxy is characterized by several relatively bright components (clumps) in a galaxy. We here consider galaxies with more than two such clumps ($N_{\rm clump} \geq 3$) as clumpy galaxies. In order to select clumpy galaxies, we first detected galaxies on the $I_{\rm F814W}$-band data, using the SExtractor software (Bertin & Arnouts 1996). A detection threshold of 2.0 times the local background root mean square over 15 connected pixels was used. We adopted the *DEBREND_NTHRESH* parameter of 64 and the *DEBLEND_MINCONT* parameter of 0.1 in the first SExtractor run. We then searched counterparts of our sample galaxies mentioned above on the $I_{\rm F814W}$-band image, and found the counterparts for 24027 galaxies out of 24176 galaxies with $I_{\rm F814W} < 22.5$ at $0.2 < z < 1.0$. Next, we changed the *DEBLEND_MINCONT* parameter to 0.001 and rerun the SExtractor to more aggressively deblend each galaxy and detect relatively bright clumps in the galaxy. The resulting catalog in this second SExtractor run was cross-matched with that in the first run. We then selected sample galaxies which are deblended into more than two components as clumpy galaxy candidates. In order to ensure that at least three clumps are comparatively bright, we set further criteria for clumpy galaxies as

$$f_2/f_1 \geq 0.3, \quad (1)$$

and

$$f_3/f_2 \geq 0.3, \quad (2)$$

where f_1, f_2, and f_3 are $I_{\rm F814W}$-band fluxes of the brightest, the second brightest, and the third brightest clumps, respectively, in the galaxy. In Figure 1, we show examples of galaxies with more than two clumps as a function

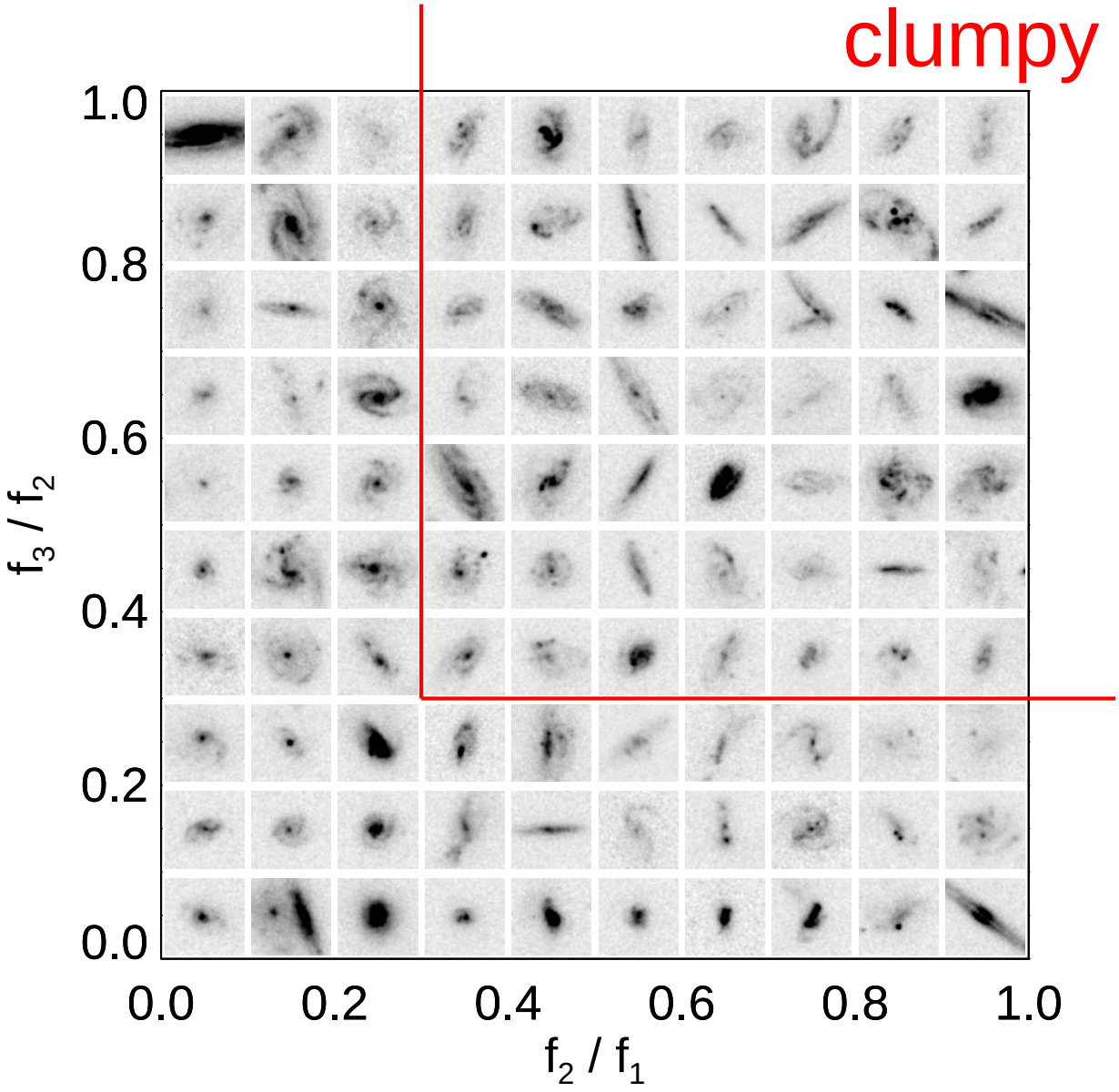

FIG. 1.— *HST*/ACS $I_{\rm F814W}$-band images of galaxies with more than two components as a function of the flux ratios among the brightest three clumps in each galaxy. f_2/f_1 is the ratio between the second brightest and the brightest clumps, while f_3/f_2 is that between the third and second brightest clumps. The red line shows the criteria for clumpy galaxies ($f_2/f_1 \geq 0.3$ & $f_3/f_2 \geq 0.3$). These galaxies are randomly selected from those with each range of the parameters.

of these flux ratios among the brightest three clumps to demonstrate our classification. One can see that our selection enable to pick up sources with several significant clumps. On the other hand, galaxies with one dominant component, which corresponds to a bulge in some cases, lie at the left side in the figure, while those with only two bright components are located at the bottom right. In this paper, we refer to all galaxies which are not satisfied by the criteria for clumpy galaxies as "non-clumpy" galaxies.

Figures 2 and 3 show examples of clumpy and non-clumpy galaxies in each redshift bin, respectively. We selected total 2803 clumpy galaxies at $0.2 < z < 1.0$ with $I_{\rm F814W} < 22.5$. Our sample sizes are summarized in Table 1.

3. RESULTS

3.1. *Stellar Mass and SFR of Clumpy Galaxies*

We show the $M_{\rm star}$–SFR diagram for the clumpy and non-clumpy galaxies, respectively, in Figure 4. Rela-

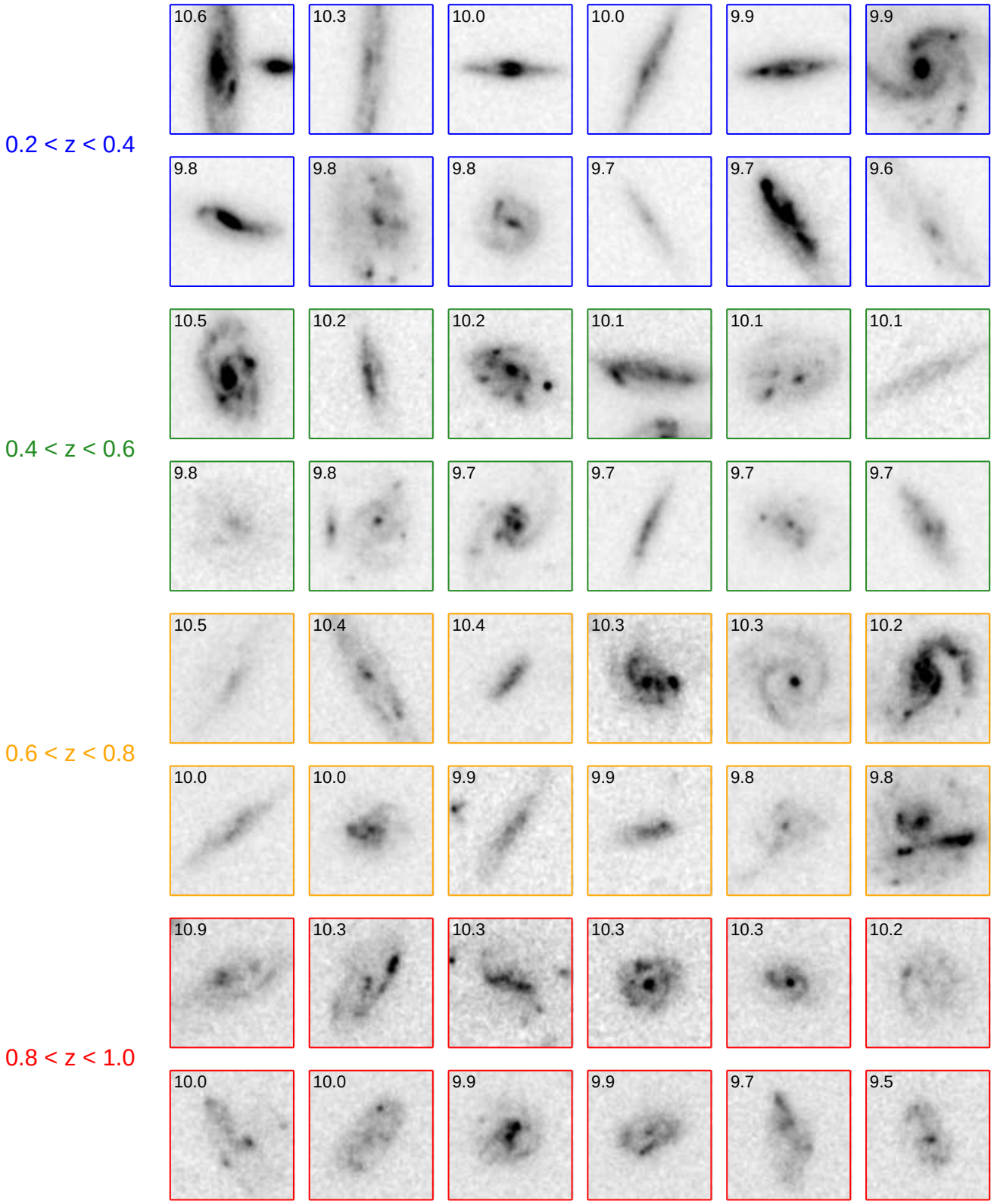

FIG. 2.— Examples of clumpy galaxies in the redshift bins. Galaxies are randomly selected in each redshift bin and are shown in the order of their stellar mass. The number in each panel shows $\log(M_{\rm star}/M_{\odot})$.

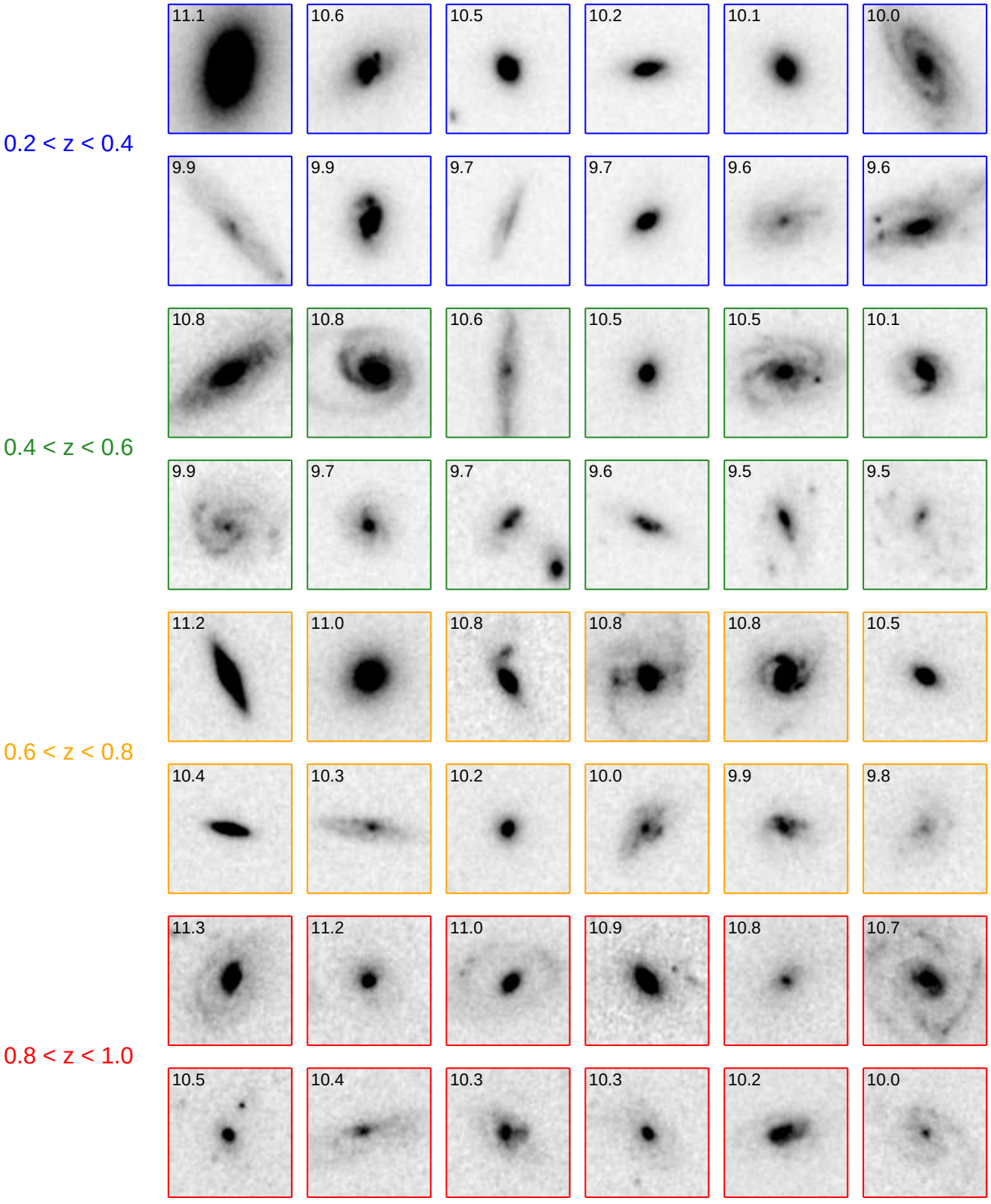

FIG. 3.— The same as Figure 2 but for non-clumpy galaxies.

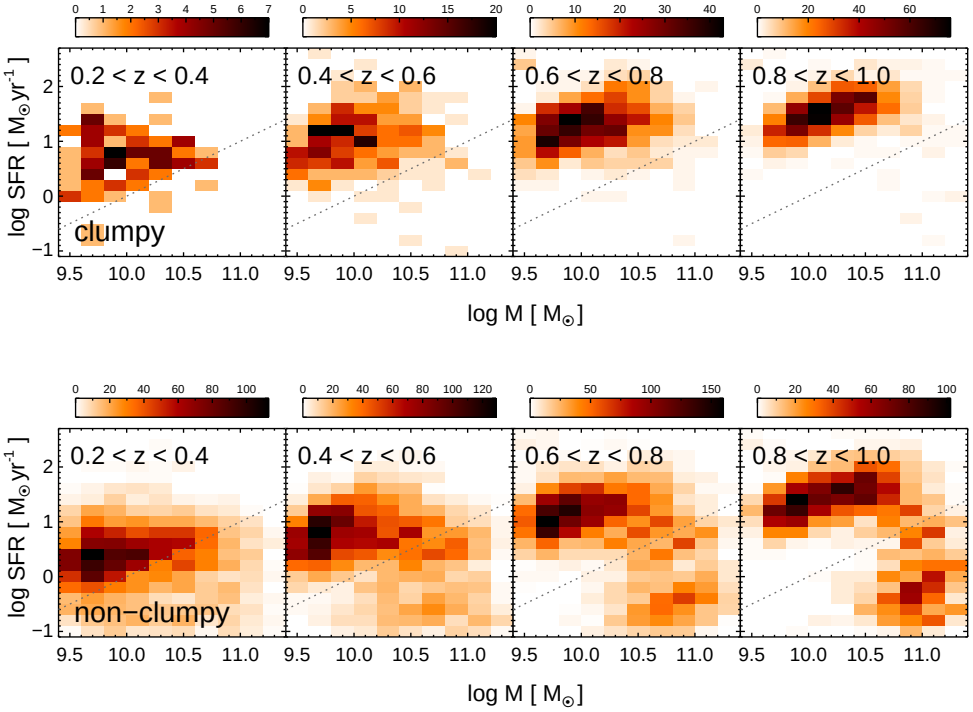

FIG. 4.— SFR vs. stellar mass for clumpy galaxies (top panels) and non-clumpy galaxies (bottom panels) in each redshift bin. The dashed line shows a constant SSFR of 0.1 Gyr^{-1}, above which galaxies are classified as star-forming ones.

tively small number of galaxies around $M_{\mathrm{star}} \sim 10^{9.5} M_{\odot}$ in the both samples is due to the magnitude limit of $I_{\mathrm{F814W}} < 22.5$. Since the observed I_{F814W} band samples a shorter rest-frame wavelength at higher redshift, low-mass galaxies with lower SFRs in the high redshift bins tend to be missed by this magnitude limit. We discuss possible systematic effects of the magnitude limit on our results in Section 3.3.

The distribution of non-clumpy galaxies in the $\mathrm{M_{star}}$–SFR diagram shows a bimodality, which consists of passively evolving galaxies mainly located at higher stellar mass around $M_{\mathrm{star}} \sim 10^{11} M_{\odot}$ and star-forming galaxies located at $M_{\mathrm{star}} \lesssim 10^{10.5} M_{\odot}$. The SFRs of star-forming galaxies increase with increasing stellar mass, and they form a sequence in the $\mathrm{M_{star}}$–SFR plane, namely, the "main sequence" of star-forming galaxies (e.g., Noeske et al. 2007). The SFRs of star-forming galaxies at a given stellar mass increase with increasing redshift over $0.2 < z < 1.0$. Such distribution of galaxies in the $\mathrm{M_{star}}$–SFR plane and its evolution at $z \lesssim 1$ are consistent with previous studies (e.g., Noeske et al. 2007; Santini et al. 2009; Kajisawa et al. 2010).

On the other hand, the clumpy galaxies are preferentially located on the main sequence of star-forming galaxies. In Figure 4, we plot the boundary line of the $SFR/M_{\mathrm{star}} = 0.1$ Gyr^{-1}, which divides galaxies into the passively evolving and star-forming populations, for reference. Since almost all clumpy galaxies lie above the boundary line, especially, at high redshift, they are star-forming galaxies. The range of the SFRs of clumpy galaxies at a given stellar mass is similar to that of the other star-forming galaxies in all the mass and redshift ranges, although their SFRs tend to be higher values as we will show in detail in the following subsection.

3.2. *Fraction of Clumpy Galaxies as a Function of Physical Properties*

We investigated the fraction of clumpy galaxies in our sample at $0.2 < z < 1.0$ as a function of stellar mass, SFR, and specific SFR (= $\mathrm{SFR/M_{star}}$, hereafter SSFR), to study their role in the galaxy evolution and the origins of their morphology. Figure 5 shows the fraction of clumpy galaxies in star-forming galaxies with $SSFR > 0.1$ Gyr^{-1} as a function of stellar mass for the different redshift bins. The fraction does not strongly depend on stellar mass in all the redshift bins, although it tends to be slightly lower at $M_{\mathrm{star}} > 10^{10.5} M_{\odot}$. We also note that the fraction at $0.8 < z < 1.0$ becomes slightly higher around $M_{\mathrm{star}} \sim 10^{10} M_{\odot}$. In Figure 4 we can see a concentration of clumpy galaxies at $M_{\mathrm{star}} \sim 10^{10} M_{\odot}$ and $SFR \sim 10^{1.75} M_{\odot}$ yr^{-1}, and therefore some fluctuation in the number density of such galaxies in our survey field may cause such high fraction of clumpy galaxies around $M_{\mathrm{star}} \sim 10^{10} M_{\odot}$ at $0.8 < z < 1.0$. There may also be the effect of the bias for galaxies with relatively high SSFR near the limiting mass at high redshift caused by the magnitude limit of $I_{\mathrm{F814W}} < 22.5$, as we show in Section 3.3. The fraction of clumpy galaxies decreases with time from ~ 0.35 at $0.8 < z < 1.0$ to ~ 0.05 at $0.2 < z < 0.4$. This is consistent with the results in the previous studies that bright clumpy galaxies are rare in the present universe, while many such galaxies have been observed at $z \gtrsim 1$ (e.g., Elmegreen et al. 2007; Elmegreen et al. 2009b).

We show the fraction of clumpy galaxies in star-forming galaxies with $SSFR > 0.1$ Gyr^{-1} as a func-

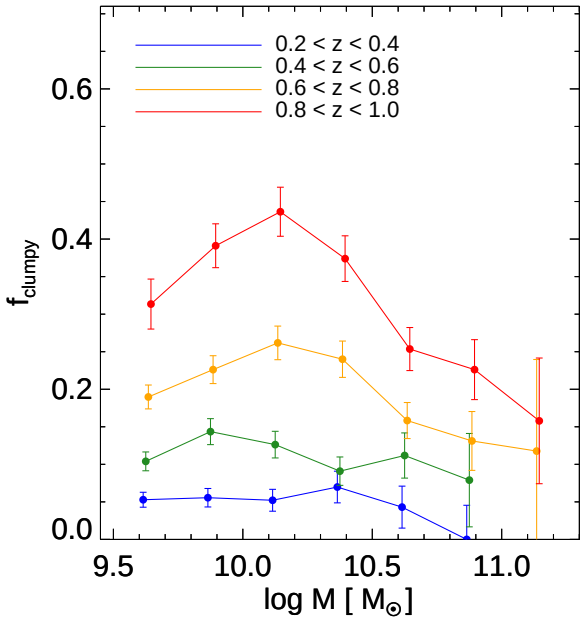

FIG. 5.— Fraction of clumpy galaxies in star-forming galaxies with $SSFR > 0.1$ Gyr^{-1} as a function of stellar mass for the different redshift bins. The error bars are based on the Poisson statistics.

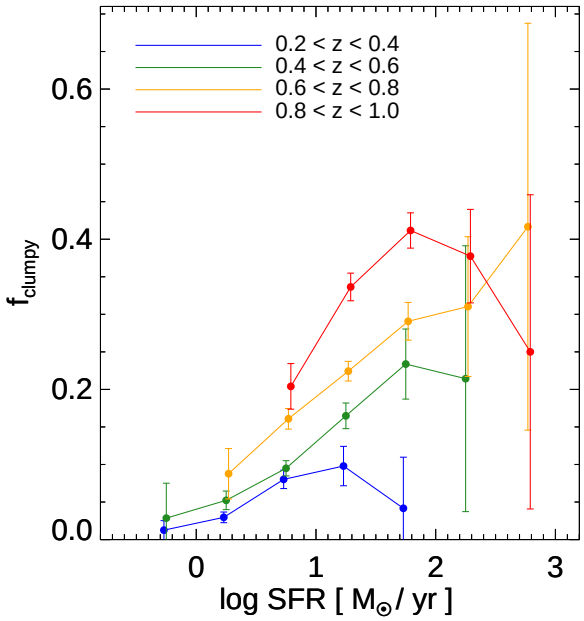

FIG. 6.— Fraction of clumpy galaxies in star-forming galaxies with $M_{\rm star} > 10^{9.5} M_{\odot}$ as a function of SFR for the different redshift bins. The error bars are based on the Poisson statistics.

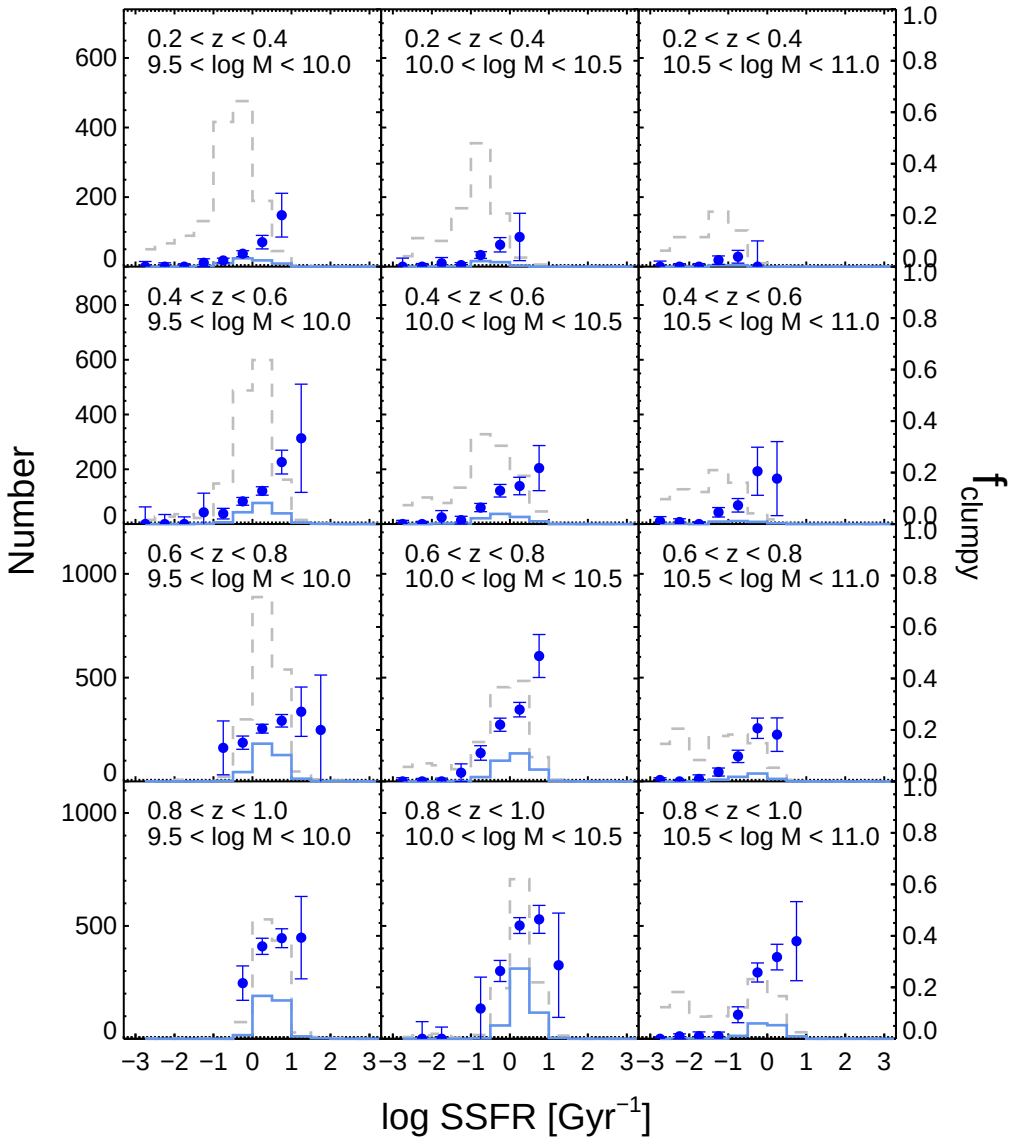

FIG. 7.— SSFR distribution for clumpy and non-clumpy galaxies (histograms) for each redshift and stellar mass bin. The fraction of clumpy galaxies is also shown as a function of SSFR (solid circles, right ordinate). The solid histogram shows clumpy galaxies, while the dashed histogram represents non-clumpy galaxies. The error bars are based on the Poisson statistics.

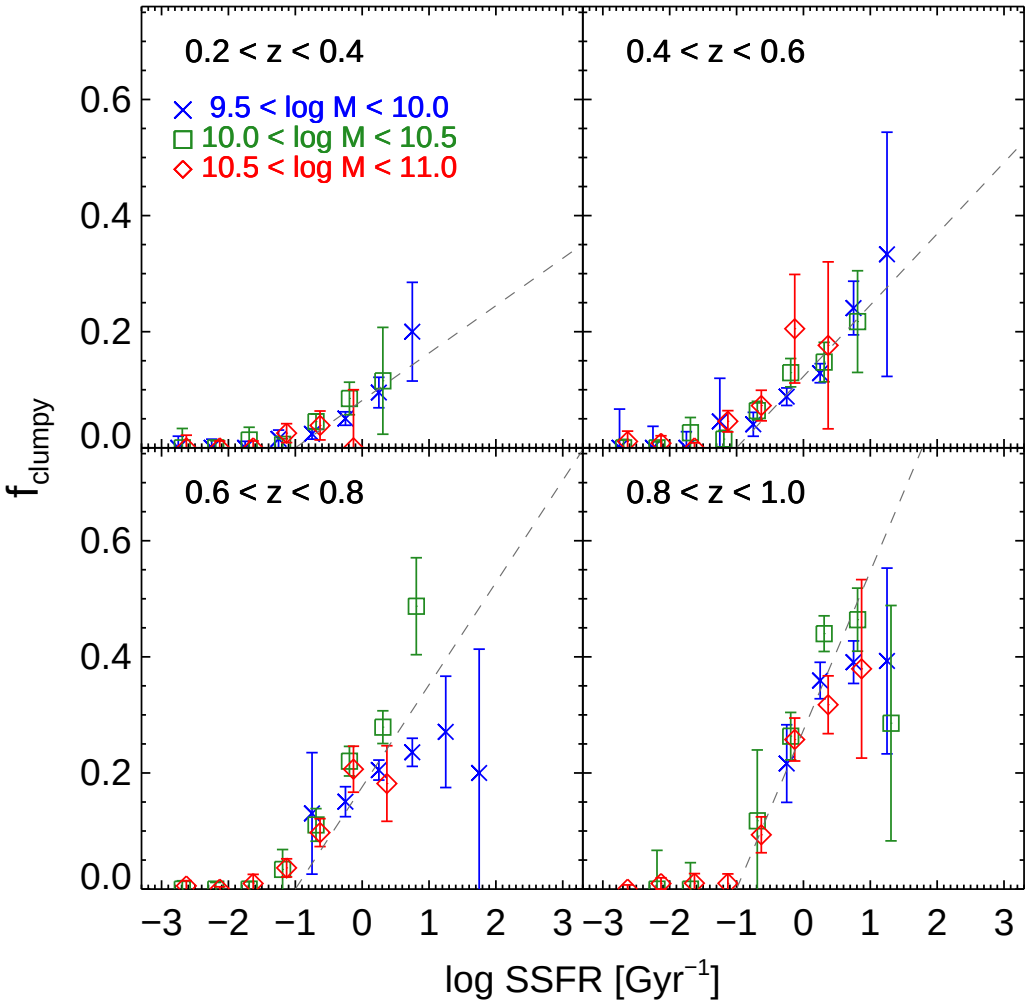

FIG. 8.— Fraction of clumpy galaxies as a function of SSFR for each redshift bin. The fractions for the different stellar mass ranges are shown in the same panel. The dashed line represents the fitting result of the data points at $SSFR > 0.1$ Gyr^{-1} with a linear line of $f_{\rm clumpy} = a \times [\log(SSFR) + 1.0]$, where a is a free parameter.

tion of SFR in Figure 6. It is shown that the fraction of clumpy galaxies clearly increases with increasing SFR in all the redshift ranges. The fraction at a given SFR decreases with time over the wide range of SFR, although the strength of the evolution seems to depend on SFR. The fraction at $SFR \sim 10^{1.75} M_\odot$ yr^{-1} decreases from ~ 0.4 at $0.8 < z < 1.0$ to ~ 0.05 at $0.2 < z < 0.4$, while that at $SFR \sim 10^{0.75} M_\odot$ yr^{-1} changes from ~ 0.2 to ~ 0.07 in the same redshift range. A slightly higher fraction around $SFR \sim 10^{1.75} M_\odot$ yr^{-1} for galaxies at $0.8 < z < 1.0$ probably corresponds to that at $M_{\rm star} \sim 10^{10} M_\odot$ in Figure 5 mentioned above.

Furthermore, we investigated the fraction of clumpy galaxies as a function of SSFR in each mass and redshift range. Figure 7 shows the SSFR distribution and the fraction of clumpy galaxies as a function of SSFR. In this figure, we used all sample galaxies, including galaxies with $SSFR < 0.1$ Gyr^{-1}. While the range of SSFRs of clumpy galaxies is similar to that of the other (non-clumpy) star-forming galaxies as shown in Figure 4, the distribution of SSFR of clumpy galaxies tends to be skewed toward higher values. In fact, the fraction of clumpy galaxies clearly increases with increasing SSFR in all the stellar mass and redshift ranges. Interestingly, we found that the fraction at a given SSFR is nearly independent of stellar mass in each redshift bin. In Figure 8, we show the fraction of clumpy galaxies as a function of SSFR for the different mass ranges in the same panel. The SSFR dependences of the fractions for the different stellar mass ranges are similar in each redshift bin, although the uncertainty of each data point is relatively large, especially at very high SSFR. In all the redshift ranges, we can see that the fraction increases with SSFR at $SSFR > 0.1$ Gyr^{-1}, while it is negligible at $SSFR < 0.1$ Gyr^{-1}. We can also see that the fraction of clumpy galaxies at a given SSFR decreases with time. For example, the fraction at $SSFR \sim 1$ Gyr^{-1} changes from ~ 0.3 at $0.8 < z < 1.0$ to ~ 0.07 at $0.2 < z < 0.4$,

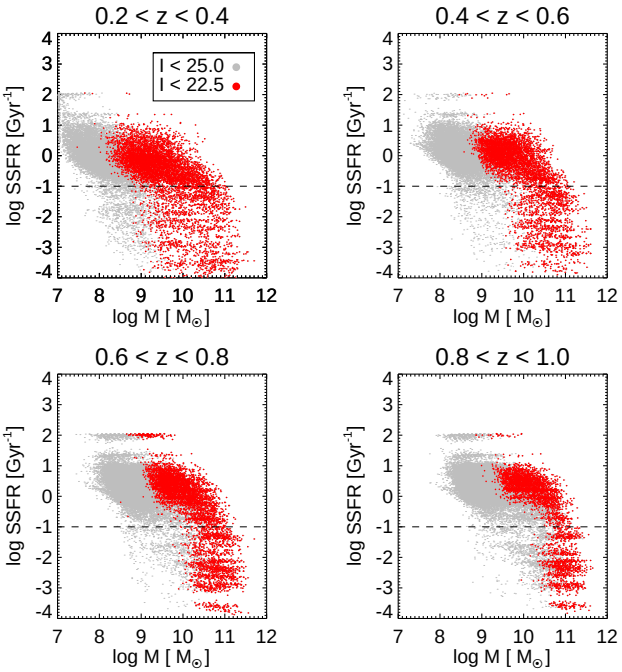

FIG. 9.— SSFR vs. stellar mass for galaxies with $I_{\rm F814W} < 22.5$ (red dots) and for those with $I_{\rm F814W} < 25.0$ (grey dots) for each redshift bin.

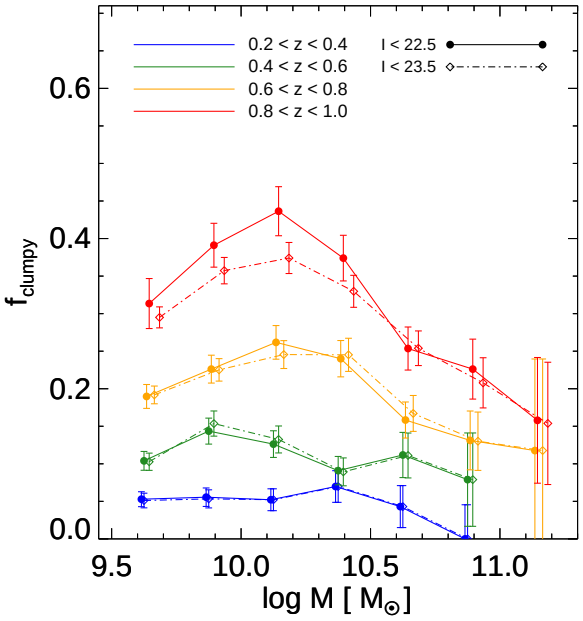

FIG. 10.— The same as Figure 5, but the results for galaxies with $I_{\rm F814W} < 23.5$ are also shown (dashed-dotted lines) as well as those for the basic sample with $I_{\rm F814W} < 22.5$ (solid lines).

while that at $SSFR \sim 10$ Gyr^{-1} decreases from ~ 0.4 to ~ 0.15 in the same redshift range. We fit the data points at $SSFR > 0.1$ Gyr^{-1} in each panel of Figure 8 with a linear line of $f_{\rm clumpy} = a \times [\log(SSFR) + 1.0]$, which satisfies $f_{\rm clumpy} = 0$ at $\log(SSFR) = -1$ (the dashed lines in the figure). The best-fit slope of the linear line on the $f_{\rm clumpy}$ – log(SSFR) plane clearly becomes steeper with redshift. Therefore, the fraction of clumpy galaxies at a given SSFR does not depend on stellar mass at each redshift, but evolves with time from $z \sim 1$ to $z \sim 0.2$.

3.3. *Possible Biases in Our Analysis*

In this section, we checked the effects of possible biases on our results in the previous subsections. First, we considered the effects of our magnitude limit of $I_{\rm F814W} < 22.5$, which is set to ensure a secure selection of clumpy galaxies. Since the observed $I_{\rm F814W}$ band samples the rest-frame B band at $z \sim 0.9$, the relatively bright $I_{\rm F814W}$-band magnitude limit can lead to a bias for galaxies with higher SSFRs at lower stellar mass. Therefore we may preferentially miss low-mass galaxies with relatively low SSFRs at higher redshift. In order to check this point in more detail, we show the SSFR-$M_{\rm star}$ diagram for galaxies with $I_{\rm F814W} < 22.5$ and those with $I_{\rm F814W} < 25$ in Figure 9. It is shown that galaxies with relatively low SSFRs are missed by the $I_{\rm F814W}$-band magnitude limit at $M_{\rm star} \lesssim 10^{10} M_\odot$ in the $0.8 < z < 1.0$ bin, while almost all galaxies with $SSFR > 0.1$ Gyr^{-1} are picked up down to $M_{\rm star} \sim 10^{9.5} M_\odot$ at lower redshifts. In Figure 10, we show the fraction of clumpy galaxies in star-forming galaxies as in Figure 5 but for galaxies with $I_{\rm F814W} < 23.5$. It is shown that the relatively high fraction around $M_{\rm star} \sim 10^{10} M_\odot$ for galaxies at $0.8 < z < 1.0$ seen in Figure 5 becomes lower, and the fraction is consistent with a constant value of ~ 0.3. This is because we include low-mass galaxies with relatively low SSFRs at high redshift by using galaxies down to $I_{\rm F814W} = 23.5$. Although we can mitigate the bias against low-mass galaxies with low SSFRs by including more faint galaxies into the sample, we note that the selection of clumpy galaxies becomes less secure for galaxies at $I_{\rm F814W} > 22.5$. On the other hand, the bias caused by the $I_{\rm F814W}$-band magnitude limit does not seem to affect the results in Figures 7 and 8, because the fraction of clumpy galaxies *at a given SSFR* is not changed by this effect. In fact, we performed the same analysis by using the different $I_{\rm F814W}$-band magnitude limits and confirmed that the trends seen in Figures 7 and 8 do not depend on the magnitude limit.

Second, we examined the effect of the morphological K-correction in our analysis. Since we selected our clumpy galaxies in the HST/ACS $I_{\rm F814W}$-band images, the morphological selection was done at the rest-frame R band at $z \sim 0.3$, while galaxies at $z \sim 0.9$ were classified at the rest-frame B band. If the clumps tend to be more conspicuous in shorter wavelengths (e.g., Elmegreen et al. 2009a; Wuyts et al. 2012; see also Guo et al. 2012), our ability to select clumpy galaxies could be weaker at lower redshifts. In order to check this effect, we performed the same selection of clumpy galaxies at $0.3 < z < 0.5$, using HST/ACS $V_{\rm F606W}$-band images, which correspond to the rest-frame B band for these galaxies. The $V_{\rm F606W}$-band data were obtained in the CANDELS survey (Grogin et al. 2011; Koekemoer et al. 2011) and cover a field of ~ 260 arcmin^2 in the COSMOS field. Although the area is $\sim$3.6% of the 1.64 deg^2 field of the $I_{\rm F814W}$-band data, we can roughly estimate the effect of the morphological K-correction. For ~ 100 star-forming galaxies with $SSFR > 0.1$ Gyr^{-1} at $0.3 < z < 0.5$, we performed the same morphological analysis with the

$V_{\rm F606W}$-band data and found that the fraction of clumpy galaxies increases from ~ 0.1 at the rest-frame V band (the observed $I_{\rm F814}$ band) to ~ 0.3–0.4 at the rest-frame B band. Wuyts et al. (2012) also pointed out that the morphological K-correction significantly affects the fraction of clumpy galaxies at $z \sim 2$. Taking account of these results, we keep in mind the effect of the morphological K-correction when discussing the evolution of the fraction of clumpy galaxies in the following section.

4. DISCUSSION

In this study, we constructed a large sample of clumpy galaxies at $0.2 < z < 1.0$ in the COSMOS field using the *HST*/ACS data and investigated the fraction of these galaxies and its evolution as a function of stellar mass, SFR, and SSFR. This is the first systematic search for clumpy galaxies at $z < 1$. Our main results are as follows.

- The fraction of clumpy galaxies in star-forming galaxies decreases with time from ~ 0.35 at $0.8 < z < 1.0$ to ~ 0.05 at $0.2 < z < 0.4$ irrespective of stellar mass, although the fraction tends to be slightly lower at $M_{\rm star} > 10^{10.5} M_{\odot}$ in each redshift bin.

- The fraction of clumpy galaxies increases with increasing both SFR and SSFR in all the redshift ranges we investigated. In particular, the SSFR dependences of the fractions are similar among galaxies with different stellar masses. Moreover, the fraction at a given SSFR does not depend on stellar mass in each redshift bin.

- The fraction of clumpy galaxies at a given SSFR decreases with time at $SSFR > 0.1$ Gyr^{-1}. This can be explained by the effect of the morphological K-correction.

We discuss these results and their implications for both origins and evolution of clumpy galaxies in the following subsections.

4.1. *SSFR dependence of the fraction of clumpy galaxies*

We found that the fraction of clumpy galaxies increases with increasing both SFR and SSFR. The similar fractions at a given SSFR among galaxies with different stellar masses may indicate that the SSFR is more important and fundamental physical parameter for the origin of the clumpy morphology. Among previous studies on clumpy galaxies, Bournaud et al. (2012) studied 14 clumpy galaxies and 13 smooth disk galaxies at $z \sim 0.7$ selected by an eyeball classification, and found that the average and median SSFRs of clumpy galaxies are higher than those of smooth disk galaxies. Salmi et al. (2012) also reported that clumpy galaxies at $0.5 < z < 1.3$ have systematically higher SSFRs than the other star-forming galaxies at the same redshifts. They selected clumpy galaxies with a quantitative clumpiness parameter, but their measurement of the clumpiness includes the surface brightness fluctuation on relatively small scales. The SSFR dependence of the fraction of clumpy galaxies seen in Figure 7 is consistent with the results of these previous studies, although the selection methods for clumpy galaxies are different among the studies.

Since the SSFR is a current birth rate of stars relative to the integrated past star formation rate, it can be considered to represent the evolutionary stages of the stellar mass assembly by the star formation. In this view, the relatively high SSFRs of clumpy galaxies indicates that these galaxies may be systematically in younger stages in their star formation history. We can also consider the SSFR as a proxy for the gas mass to stellar mass ratio, $\rm M_{gas}/M_{star}$, if we naively assume that the SFRs of galaxies roughly reflect their gas mass. Clumpy galaxies are expected to be (probably young) objects with relatively high gas mass fraction in this case. Recently, the gravitational instability and fragmentation in gas-rich disks is often proposed as a possible origin of the clumpy morphology of high-redshift galaxies, which show both coherent rotation and relatively large velocity dispersion in their gas (e.g., Immeli et al. 2004; Bournaud et al. 2007; Dekel et al. 2009a; Bournaud et al. 2010; Genzel et al. 2012). Gas-rich rotational disks are gravitationally unstable for the fragmentation and lead to the formation of large clumps. In this framework, the gas mass fraction is a key physical parameter. The stability for the gravitational fragmentation of the disks and the maximum unstable mass scale strongly depend on the gas mass fraction (e.g., Escala & Larson 2008; Cacciato et al. 2012). If the SSFR is closely related to the gas mass fraction, the strong SSFR dependence of the fraction of clumpy galaxies in Figure 7 can be explained by the relationship between the gravitational fragmentation and the gas mass fraction of the rotational disks.

Escala (2011) also discussed that a large maximum unstable mass of gas-rich disks corresponds to a large velocity dispersion of turbulent motions of gas in the self-regulated quasi-stationary state with the Toomre parameter $Q \sim 1$. They also claimed that the large velocity dispersion can cause an enhancement of star formation activity. In fact, the correlation between the mass of the most massive clump of galaxies and their surface SFR density has been observed at $z \gtrsim 1$ (Livermore et al. 2012; Swinbank et al. 2012). This scenario may explain the relatively higher SSFRs of clumpy galaxies.

Another possible origin of the clumpy morphology is the galaxy merger (e.g., Somerville et al. 2001; Lotz et al. 2004). For example, Di Matteo et al. (2008) performed extensive numerical simulations of major mergers and found that gas-rich major mergers can cause the greater disk fragmentation than the cases of isolated gas-rich galaxies. Morphological studies of high-redshift galaxies and comparisons of these objects with merger galaxies in the nearby universe suggested that some fraction of clumpy and irregular galaxies at $z \gtrsim 1$ are ongoing mergers (e.g., Lotz et al. 2008; Petty et al. 2009; Overzier et al. 2010). Mandelker et al. (2013) suggested that a non-negligible fraction of large clumps in high-redshift clumpy galaxies come from minor mergers, based on a numerical cosmological simulation of disk galaxies. Puech (2010) reported that a significant fraction of intermediate-mass clumpy galaxies at $z \sim 0.6$ have complex kinematics, which is compatible with major mergers. In this scenario, the SSFR dependence of the fraction of clumpy galaxies can be understood by the enhancement of star formation caused by the galaxy mergers. The galaxy interaction/merger does not only cause disturbed and clumpy morphologies, but also trig-

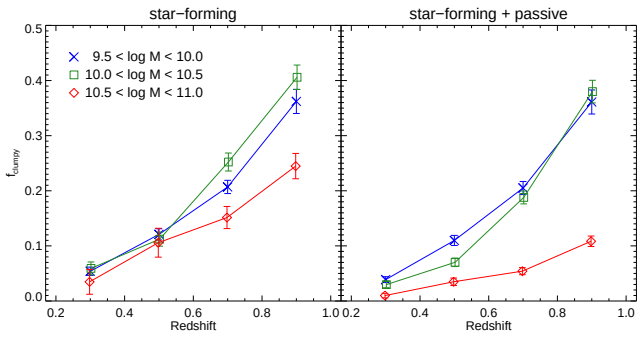

FIG. 11.— **left:** Evolution of the fraction of clumpy galaxies in star-forming galaxies ($SSFR > 0.1$ Gyr^{-1}) with different stellar masses. **right:** The same as the left panel but for all galaxies with $I_{\rm F814W} < 22.5$ including passively evolving galaxies.

gers intense star formation. Thus the SSFRs of clumpy galaxies tend to be enhanced from the main sequence of star-forming galaxies. However, it is unclear whether such starbursts by mergers are consistent with the relatively tight SFR-$M_{\rm star}$ relation or not (e.g., Noeske et al. 2007; Elbaz et al. 2007; Renzini 2009; Wuyts et al. 2011; Rodighiero et al. 2011).

4.2. *Evolution of the fraction of clumpy galaxies*

We found that the overall fraction of clumpy galaxies in star-forming galaxies with $M_{\rm star} > 10^{9.5} M_\odot$ decreases from ~ 0.35 at $z \sim 0.9$ to ~ 0.05 at $z \sim 0.3$. While many actively star-forming galaxies with clumpy morphologies have been observed at $z > 1$ (e.g., Elmegreen et al. 2007; Genzel et al. 2008; Förster Schreiber et al. 2011), most relatively bright galaxies belong to the Hubble sequence and clumpy galaxies are very rare at $z \sim 0$ (e.g., Overzier et al. 2010). Our result naturally connects between these previous studies in the early universe and those in the nearby universe, although the morphological K-correction may affect the result (Section 3.3). Wuyts et al. (2012) reported that the fraction of clumpy galaxies in star-forming galaxies at $z \sim 1$ is 27 % when the selection for clumps was performed at the rest-frame V band. Our result at $0.8 < z < 1.0$ ($\sim 30\%$), which was obtained at the rest-frame B band (see Section 3.3), is consistent with their result, although the selection criteria for clumpy galaxies are different.

Several authors pointed out that the clumpy morphology persists to lower redshifts in lower-mass galaxies, so called "down-sizing effect" in the clumpy morphology (e.g., Elmegreen et al. 2009b; Elmegreen 2011). There are many bright/massive clumpy galaxies at $z \gtrsim 1$, while such clumpy morphology can be seen only in low-mass systems such as dwarf irregular galaxies in the present universe. In Figure 11, we show the evolution of the fraction of clumpy galaxies with different stellar masses in order to investigate the down-sizing effect. The evolution is similar among the different mass samples, while the fraction of clumpy galaxies is slightly lower in massive galaxies with $M_{\rm star} > 10^{10.5} M_\odot$. The differences of the fraction among galaxies with different masses become larger when we include passive galaxies with $SSFR < 0.1$ Gyr^{-1} into the samples (the right panel of Figure 11). If we extrapolate the trend in Figure 11 to the present, the fraction of clumpy galaxies in more massive galaxies

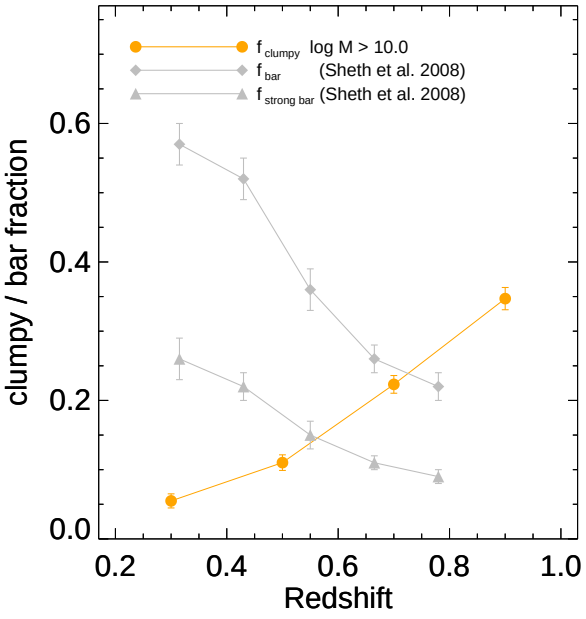

FIG. 12.— Fraction of clumpy galaxies in star-forming galaxies with $M_{\rm star} > 10^{10} M_\odot$ and the fractions of barred spiral galaxies from Sheth et al. (2008) as a function of redshift. Diamonds show the fraction of all barred spiral galaxies, while triangles represent that of strong barred galaxies. These fractions of barred galaxies are measured in face-on spiral galaxies with inclination angles of $i > 65°$ (see Sheth et al. 2008 for details).

is expected to become negligible earlier. Therefore, our result is not inconsistent with the down-sizing picture, but the mass dependence of the evolution is weak in the stellar mass range we investigated. The lower fraction of clumpy galaxies in massive star-forming galaxies with $M_{\rm star} > 10^{10.5} M_\odot$ at each redshift may be explained by lower SSFR of these massive galaxies (Figure 9).

Another our result of the SSFR dependence of the fraction of clumpy galaxies seen in all the mass and redshift ranges indicates that the evolution of the SSFRs of galaxies leads to the evolution of the fraction of clumpy galaxies. In fact, the median SSFR of star-forming galaxies decreases by ~ 1 dex from $z \sim 0.9$ to $z \sim 0.3$ (Figure 7). For example, if we assume the relation between the fraction of clumpy galaxies and SSFR at $0.8 < z < 1.0$ shown in Figure 8, the decrease of the SSFR from $SSFR \sim 10^{0.25}$ Gyr^{-1} (median value at $z \sim 0.9$) to $SSFR \sim 10^{-0.75}$ Gyr^{-1} (that at $z \sim 0.3$) corresponds to the evolution of the fraction from ~ 0.35 to ~ 0.05. Thus the evolution of the fraction of clumpy galaxies in star-forming galaxies at $0.2 < z < 1.0$ appear to be explained by the evolution of the SSFR. On the other hand, from such correlation between the fraction of clumpy galaxies and SSFR, the fraction of clumpy galaxies is expected to be higher at higher redshifts, because galaxies tend to have higher SSFRs than those at $z \lesssim 1$. Wuyts et al. (2012) found that the fraction of clumpy galaxies in star-forming galaxies with $M_{\rm star} > 10^{10} M_\odot$ at $1.5 < z < 2.5$ is 42% when the morphological selection was done at the rest-frame V band. Tadaki et al. (2014) also reported that 42% of Hα emitters at $z \sim 2.2$ and 2.5 have clumpy morphology, although their clump selec-

tion was performed with both rest-frame UV and optical-bands images. The average SSFRs of star-forming galaxies at $z \sim 2$ in both studies are $\sim 10^{0.5}$ Gyr^{-1}, and therefore the fractions of clumpy galaxies of $\sim 40\%$ in these studies seem to be consistent with the relation between the fraction of clumpy galaxies and SSFR at $0.8 < z < 1.0$ shown in Figure 8.

In the gravitational fragmentation model for the formation of giant clumps in disk galaxies, the rapid and smooth streams of gas along filaments effectively penetrate halos of galaxies at high redshift (e.g., Kereš et al. 2005; Dekel et al. 2009b). This "cold accretion" keeps active star formation and a high gas mass fraction of these galaxies, which leads to the formation of the clumpy morphology. In fact, such high gas mass fraction of star-forming galaxies at $z \sim 2$ have been observed (e.g., Daddi et al. 2010; Tacconi et al. 2013), and the observed high turbulent velocity of gas in high-redshift clumpy galaxies also supports this scenario (e.g., Cresci et al. 2009; Förster Schreiber et al. 2009). Using an analytic model, Cacciato et al. (2012) predicted that such disks tend to stabilize at $z \lesssim 1$ mainly due to the decrease of the gas mass fraction. They suggested that the decrease is attributed to the gradual decline of the cosmological accretion rate into halos of galaxies with time (e.g., Genzel et al. 2008), the gas consumption by the star formation, the inflows of clumps into the center of galaxies by the gravitational torque (e.g, Dekel et al. 2009a), and the gas outflows by the supernova feedback. If the SSFRs of galaxies are closely related to the gas mass fraction as discussed above, the evolution of the fraction of clumpy galaxies at $0.2 < z < 1.0$ could be explained by this scenario. The decrease of the gas mass fraction with time at $z \lesssim 1$ causes the stabilization of galactic disks, while it also leads to the decrease of the SSFRs of these galaxies. Interestingly, several studies reported that the fraction of barred spiral galaxies increases with time in the same redshift range (e.g., Abraham et al. 1999; Sheth et al. 2008; Melvin et al. 2014). The bar instability is considered to occur in "mature"systems where stellar disk is dynamically cold and rotationally supported, and the surface stellar density is sufficiently high. Clumpy galaxies may evolve to these barred galaxies when the gas fraction becomes lower and the stellar disk is stabilized (e.g., Immeli et al. 2004; Sheth et al. 2012; Kraljic et al. 2012). In Figure 12, we compare the fraction of clumpy galaxies with the fraction of barred spiral galaxies in the same COSMOS field from Sheth et al. (2008). Note that since the bar fraction in Sheth et al. (2008) is the fraction of barred galaxies in face-on spiral galaxies with $i > 65°$ excluding irregular galaxies, it is difficult to directly compare the absolute values of the both fractions. Nevertheless, we can see the fraction of barred spiral galaxies increases with time, as the fraction of clumpy galaxies decreases in the figure. The transition from clumpy galaxies to barred spiral galaxies may gradually occur from $z \sim 1$ to $z \sim 0$.

On the other hand, in the major merger scenario for the origin of the clumpy morphology, the evolution of the major merger rate may explain the evolution of the fraction of clumpy galaxies at $0.2 < z < 1.0$. Many observational studies have found that the major merger rate decreases with time at $z \lesssim 1$ (e.g., Le Fèvre et al. 2000; Conselice et al. 2003; Lin et al. 2008; de Ravel et al. 2009; Xu et al. 2012; see also Lotz et al. 2011). In particular, several studies reported that the gas-rich wet major merger, which is considered to be important for making the clumpy morphology (Di Matteo et al. 2008), decreases with time in the redshift range (Chou et al. 2011; Puech et al. 2012; López-Sanjuan et al. 2013). Figure 13 compares the observed fraction of clumpy galaxies at $0.2 < z < 1.0$ with that expected from the wet major merger rate of galaxies with $M_{\rm star} \sim 10^{10} - 10^{10.5} M_{\odot}$ by López-Sanjuan et al. (2013). We multiplied the major merger rate from López-Sanjuan et al. (2013) by an arbitrary time scale when the merged galaxies are seen as clumpy galaxies to estimate the expected fraction of clumpy galaxies. The evolution of clumpy galaxies can be roughly explained by the evolution of the major merger rate with the time scales of $\sim$ 3–6 Gyr. However, these time scales seem to be too long for the merger time scale during which the morphology is disturbed and clumpy (e.g., Di Matteo et al. 2008; Lotz et al. 2010). If we assume a typical merger time scale of ~ 0.5 Gyr, the expected fraction of clumpy galaxies become much lower than the observed fraction at $z \gtrsim 0.5$ (the dashed line in Figure 13). It seems to be difficult to explain the fraction of clumpy galaxies at $0.2 < z < 1.0$ only by the wet major merger.

Finally, we note that the fraction of clumpy galaxies at a given SSFR decreases with time from $z \sim 0.9$ to $z \sim 0.3$. This can be due to the morphological K-correction because we selected clumpy galaxies at the observed $I_{\rm F814W}$ band as discussed in Section 3.3. If this is the case, the intrinsic fraction of clumpy galaxies at a given SSFR could not depend on redshift. There may be the universal relation between the fraction of clumpy

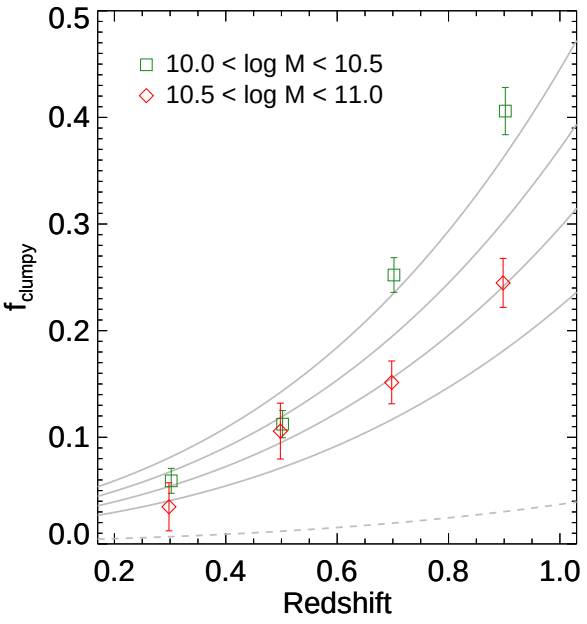

FIG. 13.— Comparison between the observed fraction of clumpy galaxies and that expected from wet major merger rate by López-Sanjuan et al. (2013). The solid lines show the major merger rate multiplied by a time scale of 3, 4, 5, and 6 Gyr, while the dashed line represents that multiplied by a time scale of 0.5 Gyr.

galaxies and SSFR.

We would like to thank the anonymous referee for valuable comments and suggestions. We also thank Tsutomu T. Takeuchi at Nagoya University for his generous support to K. L. M. and for useful discussion. The HST COSMOS Treasury program was supported through NASA grant HST-GO-09822. We greatly acknowledge the contributions of the entire COSMOS collaboration consisting of more than 70 scientists. This work was financially supported in part by the Japan Society for the Promotion of Science (Nos. 17253001, 19340046, 23244031, and 23740152).

REFERENCES

Abraham, R. G., Merrifield, M. R., Ellis, R. S., Tanvir, N. R., & Brinchmann, J. 1999, MNRAS, 308, 569
Bertin, E., & Arnouts, S. 1996, A&AS, 117, 393
Bournaud, F., Elmegreen, B. G., & Elmegreen, D. M. 2007, ApJ, 670, 237
Bournaud, F., Elmegreen, B. G., Teyssier, R., Block, D. L., & Puerari, I. 2010, MNRAS, 409, 1088
Bournaud, F., Juneau, S., Le Floc'h, E., et al. 2012, ApJ, 757, 81
Bruzual, G., & Charlot, S. 2003, MNRAS, 344, 1000
Cacciato, M., Dekel, A., & Genel, S. 2012, MNRAS, 421, 818
Calzetti, D., Armus, L., Bohlin, R. C., et al. 2000, ApJ, 533, 682
Cameron, E., Carollo, C. M., Oesch, P. A., et al. 2011, ApJ, 743, 146
Chabrier, G. 2003, PASP, 115, 763
Chou, R. C. Y., Bridge, C. R., & Abraham, R. G. 2011, AJ, 141, 87
Conselice, C. J., Bershady, M. A., Dickinson, M., & Papovich, C. 2003, AJ, 126, 1183
Cowie, L. L., Hu, E. M., & Songaila, A. 1995, AJ, 110, 1576
Cresci, G., Hicks, E. K. S., Genzel, R., et al. 2009, ApJ, 697, 115
Daddi, E., Bournaud, F., Walter, F., et al. 2010, ApJ, 713, 686
Dekel, A., Sari, R., & Ceverino, D. 2009a, ApJ, 703, 785
Dekel, A., Birnboim, Y., Engel, G., et al. 2009b, Nature, 457, 451
de Ravel, L., Le Fèvre, O., Tresse, L., et al. 2009, A&A, 498, 379
Di Matteo, P., Bournaud, F., Martig, M., et al. 2008, A&A, 492, 31
Elbaz, D., Daddi, E., Le Borgne, D., et al. 2007, A&A, 468, 33
Elmegreen, B. G. 2011, EAS Publications Series, 51, 59
Elmegreen, B. G., Elmegreen, D. M., Fernandez, M. X., & Lemonias, J. J. 2009a, ApJ, 692, 12
Elmegreen, D. M., Elmegreen, B. G., Marcus, M. T., et al. 2009b, ApJ, 701, 306
Elmegreen, D. M., Elmegreen, B. G., Ferguson, T., & Mullan, B. 2007, ApJ, 663, 734
Elvis, M., Civano, F., Vignali, C., et al. 2009, ApJS, 184, 158
Escala, A., & Larson, R. B. 2008, ApJ, 685, L31
Escala, A. 2011, ApJ, 735, 56
Förster Schreiber, N. M., Genzel, R., Lehnert, M. D., et al. 2006, ApJ, 645, 1062
Förster Schreiber, N. M., Genzel, R., Bouché, N., et al. 2009, ApJ, 706, 1364
Förster Schreiber, N. M., Shapley, A. E., Genzel, R., et al. 2011, ApJ, 739, 45
Genzel, R., Burkert, A., Bouché, N., et al. 2008, ApJ, 687, 59
Genzel, R., Tacconi, L. J., Combes, F., et al. 2012, ApJ, 746, 69
Grogin, N. A., Kocevski, D. D., Faber, S. M., et al. 2011, ApJS, 197, 35
Guo, Y., Giavalisco, M., Ferguson, H. C., Cassata, P., & Koekemoer, A. M. 2012, ApJ, 757, 120
Hasinger, G., Cappelluti, N., Brunner, H., et al. 2007, ApJS, 172, 29
Hubble, E. P. 1936, Realm of the Nebulae, by E.P. Hubble. New Haven: Yale University Press, 1936. ISBN 9780300025002,
Ilbert, O., McCracken, H. J., Le Fèvre, O., et al. 2013, A&A, 556, A55 q
Ilbert, O., Salvato, M., Le Floc'h, E., et al. 2010, ApJ, 709, 644
Ilbert, O., Capak, P., Salvato, M., et al. 2009, ApJ, 690, 1236
Immeli, A., Samland, M., Westera, P., & Gerhard, O. 2004, ApJ, 611, 20
Kajisawa, M., & Yamada, T. 2001, PASJ, 53, 833
Kajisawa, M., Ichikawa, T., Yamada, T., et al. 2010, ApJ, 723, 129
Kereš, D., Katz, N., Weinberg, D. H., & Davé, R. 2005, MNRAS, 363, 2
Koekemoer, A. M., Aussel, H., Calzetti, D., et al. 2007, ApJS, 172, 196
Koekemoer, A. M., Faber, S. M., Ferguson, H. C., et al. 2011, ApJS, 197, 36
Kraljic, K., Bournaud, F., & Martig, M. 2012, ApJ, 757, 60
Le Fèvre, O., Abraham, R., Lilly, S. J., et al. 2000, MNRAS, 311, 565
Lin, L., Patton, D. R., Koo, D. C., et al. 2008, ApJ, 681, 232
Livermore, R. C., Jones, T., Richard, J., et al. 2012, MNRAS, 427, 688
López-Sanjuan, C., Le Fèvre, O., Tasca, L. A. M., et al. 2013, A&A, 553, A78
Lotz, J. M., Primack, J., & Madau, P. 2004, AJ, 128, 163
Lotz, J. M., Davis, M., Faber, S. M., et al. 2008, ApJ, 672, 177
Lotz, J. M., Jonsson, P., Cox, T. J., & Primack, J. R. 2010, MNRAS, 404, 590
Lotz, J. M., Jonsson, P., Cox, T. J., et al. 2011, ApJ, 742, 103
Mandelker, N., Dekel, A., Ceverino, D., et al. 2013, arXiv:1311.0013
Melvin, T., Masters, K., Lintott, C., et al. 2014, MNRAS, 438, 2882
Noeske, K. G., Weiner, B. J., Faber, S. M., et al. 2007, ApJ, 660, L43
Noguchi, M. 1998, Nature, 392, 253
Overzier, R. A., Heckman, T. M., Tremonti, C., et al. 2009, ApJ, 706, 203
Overzier, R. A., Heckman, T. M., Schiminovich, D., et al. 2010, ApJ, 710, 979
Petty, S. M., de Mello, D. F., Gallagher, J. S., III, et al. 2009, AJ, 138, 362
Puech, M. 2010, MNRAS, 406, 535
Puech, M., Hammer, F., Hopkins, P. F., et al. 2012, ApJ, 753, 128
Renzini, A. 2009, MNRAS, 398, L58
Rodighiero, G., Daddi, E., Baronchelli, I., et al. 2011, ApJ, 739, L40
Salmi, F., Daddi, E., Elbaz, D., et al. 2012, ApJ, 754, L14
Santini, P., Fontana, A., Grazian, A., et al. 2009, A&A, 504, 751
Scoville, N., Aussel, H., Brusa, M., et al. 2007, ApJS, 172, 1
Sheth, K., Elmegreen, D. M., Elmegreen, B. G., et al. 2008, ApJ, 675, 1141
Sheth, K., Melbourne, J., Elmegreen, D. M., et al. 2012, ApJ, 758, 136
Somerville, R. S., Primack, J. R., & Faber, S. M. 2001, MNRAS, 320, 504
Steidel, C. C., Giavalisco, M., Dickinson, M., & Adelberger, K. L. 1996, AJ, 112, 352
Swinbank, A. M., Smail, I., Sobral, D., et al. 2012, ApJ, 760, 130
Tacconi, L. J., Genzel, R., Neri, R., et al. 2010, Nature, 463, 781
Tacconi, L. J., Neri, R., Genzel, R., et al. 2013, ApJ, 768, 74
Tadaki, K.-i., Kodama, T., Tanaka, I., et al. 2014, ApJ, 780, 77
Wright, S. A., Larkin, J. E., Barczys, M., et al. 2007, ApJ, 658, 78
Wuyts, S., Förster Schreiber, N. M., Lutz, D., et al. 2011, ApJ, 738, 106
Wuyts, S., Förster Schreiber, N. M., Genzel, R., et al. 2012, ApJ, 753, 114
Xu, C. K., Shupe, D. L., Béthermin, M., et al. 2012, ApJ, 760, 72